All-Optical Discrimination Based on Nonlinear Transmittance of MQW Semiconductor Optical Gates

Akira Hirano, Hiroyuki Tsuda, Hideki Kobayashi, Ryo Takahashi, Masaki Asobe, Kenji Sato, and Kazuo Hagimoto

Abstract—**This paper proposes an all-optical regenerator utilizing a novel all-optical discriminator. The impacts of nonlinearity of optical gates on discrimination performance are estimated. The evaluation of discrimination performance shows that amplified spontaneous emission noise and wave form distortion in optical signals can be effectively suppressed. We experimentally demonstrate the suppression using a low-temperature-grown optical switch up to 10 Gb/s.**

Index Terms—**Optical discrimination, optical gate, saturated absorber.**

I. Introduction

THE emerging demands for more transmission capacity driven by progress in multimedia services and computer networks will become more intense in the near future. Time division multiplexing is a key technique to meet the demands. In order to increase the transmission capacity of time division multiplexed system, operating speed has to be boosted beyond the bandwidth limit of electronic circuits. All-optical processing circuits are suitable for such high-speed processing because they have the potential for ultra fast response time.

In such high-speed transmission systems, accumulated amplified spontaneous emission (ASE) noise generated by erbium-doped fiber amplifiers (EDFA's) determines the signal-to-noise ratio (SNR) limit for the maximum transmission distance, if no regenerative repeaters are used. Regenerators regain the SNR. The conventional regenerator shown in Fig. 1 consists of an optical amplifier, an optoelectrical (OE) converter, electrical amplifiers, an electrical timing extractor, an electrical decision circuit, a driver amplifier, a light source, an optical intensity modulator, and an optical booster amplifier. Among these components, the key ones are the amplifier, decision circuit, and timing extractor. The decision circuit discriminates incoming data stream into the "1" and "0" level.

To achieve ultrafast all-optical regenerators, there are several optical gate [1]–[4] candidates for the optical discrimination circuits, and optical mode-locking [8] or optical phase-locked loop (PLL) circuits [9] are expected to be used as timing extractors. In this work, we focus on optical discrimination.

Manuscript received May 21, 1998; revised February 11, 1999.

A. Hirano, M. Asobe, K. Sato, and K. Hagimoto are with the NTT Optical Network Systems Laboratories, Kanagawa 239-0847 Japan.

H. Tsuda, H. Kobayashi, and R. Takahashi are with the NTT Opto-electronics Laboratories, Kanagawa 243-0198 Japan.

Publisher Item Identifier S 0733-8724(99)03816-5.

Optical discriminators using an interferometric switch based on semiconductor optical amplifiers (SOA's) or a nonlinear fiber-loop mirror (NOLM) switch have been presented recently [1]–[4]. These devices can be categorized into resonant and nonresonant types. NOLM-based switches are nonresonant types. Resonant means that optical switching is realized by the generation of actual carriers which means the operating speed is limited by the relaxation time of the carriers. On the other hand, no actual carriers are involved in nonresonant switching. Operating speed is determined by ultra fast Kerr nonlinearity, which provides the response time of several fs. In general, nonresonant-type circuits such as NOLM have relatively large latency due to its long switching fibers. In contrast, resonant-type circuits have relatively small dimensions owing to the large nonlinearity induced from carrier excitations and relaxation. Our low-temperature-grown optical switch (LCTOS) [5]–[7] is a compact resonant-type optical gate that has ultrafast carrier relaxation time.

Our target is the realization of an all-optical high-speed regeneration circuit without any optical detectors, electrical amplifiers, electrical decision circuits, or electrooptical (EO) modulators. Such a regenerator would overcome the SNR limit and suppress the penalty caused by waveform distortion without the bandwidth limitation of electrical, EO, and (OE) circuits. The all-optical discriminator (ODSC) [10]–[12] enables high-speed, simple, and compact all-optical regenerator.

In this paper, we report on a simplified evaluation of the discrimination performance of these optical gates with the introduction of performance parameters for their transmittance. We demonstrate all-optical discrimination performance utilizing LOTOS.

II. Optical Discrimination

The conceptual model of the ODSC is shown in Fig. 2. The discriminator consists of an optical amplifier, optical gate, and a local clock pulse source. The optical amplifier controls the "optical" decision level by changing its gain. The local clock pulse source generates low-noise optical clock pulses which are synchronized with the input signal pulses. The optical gate discriminates the input degraded optical signal pulses. The clock pulses are encoded by the signal pulses via nonlinear gating by the optical gate. Nonlinear change in the transmittance of the optical gate caused by amplified signal pulses encodes optical clock pulses, which are simultaneously input to the gate. Accumulated noise on the "1" and "0" level

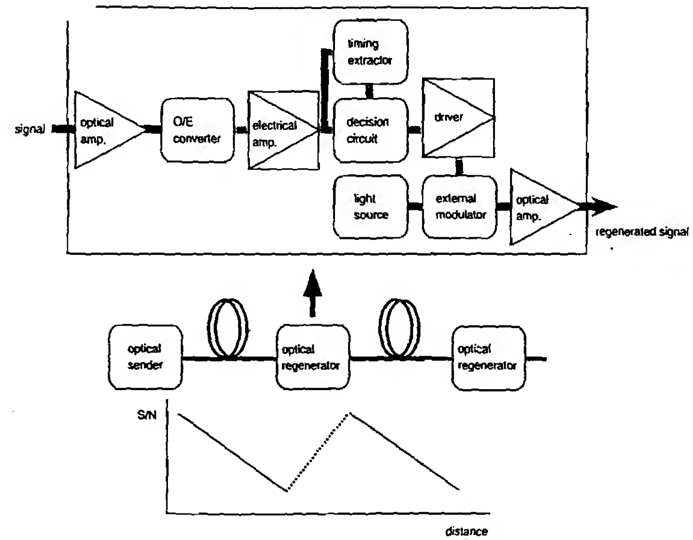

Fig. 1. Configuration of conventional optical regenerator.

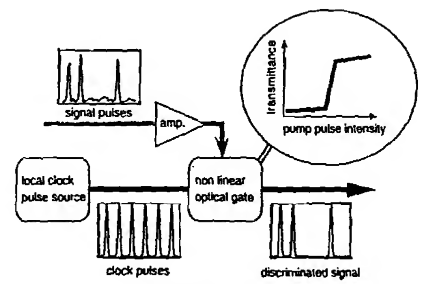

Fig. 2. Conceptual model of optical discriminator.

in incoming signal pulses transmitted through optical fiber links can be suppressed by the nonlinear gating, and the SNR of discriminated optical pulses have almost the same value as the SNR before transmission. Nonlinearity of the gates is the key feature for the discrimination performances. As for a timing jitter reduction, we must coincide temporal position of signal and clock pulses. The margin for relative delay is also an important issue [13] and will be discussed for LOTOS in Section VII. We will discuss discrimination performance in the next section.

III. Estimation of Discrimination Performance

A. Model

We used the simple model shown in Fig. 3 to evaluate the discrimination performance. The optical sender generates optical signal pulses that have shot noise only. The loss medium acts as a pure absorber and adds no additional noise. Optical amplifier α amplifies optical signal pulses and has a noise figure of 3 dB, which means inverse population factor n_{sp} is unity. We assume that the nonlinear optical gate has no loss at maximum transmittance for simplicity. Discriminated signal is received by the optical receiver, which contains an optical preamplifier β. The bit error rate was estimated for the detected signal.

B. Ideal Nonlinear Transmittance of Optical Gates

The ODSC uses optical gates that have nonlinear transmittance as a function of inputted pump pulse intensity. Transmittance is primarily determined by pump pulse energy in a resonant-type switch and by pumping peak power in a nonresonant-type. Ideal nonlinear transmittance characteristics are shown in Fig. 4. The transmittance abruptly increases at a threshold pump pulse energy. For lower pumping energy, the gate shows a high extinction ratio, and high flat transmittance for higher pumping energy. We call the threshold energy the "optical decision level." We optimize the "optical decision level" to one that gives the lowest bit error probabilities.

C. Performance Parameters for Optical Gates

For the calculation of discrimination performance, we defined the performance parameters for optical gates. Each parameter is defined as shown in Fig. 5(a), where I_{max} means the maximum pumping intensity and δI is the allowable pumping dynamic range for discrimination. $\sigma_{(0,1)t}$ and $\sigma_{(0,1)I}$ are the variances of transmittance and pumping intensity range for the (0,1) level. We define I_{th} as the pumping

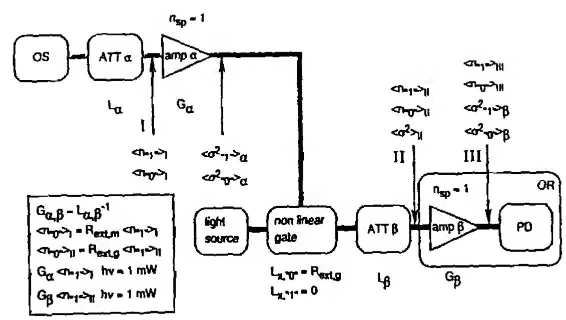

Fig. 3. Model for optical discrimination evaluation.

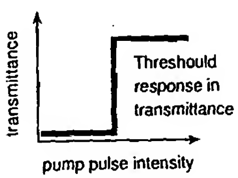

Fig. 4. Ideal dynamic transmittance.

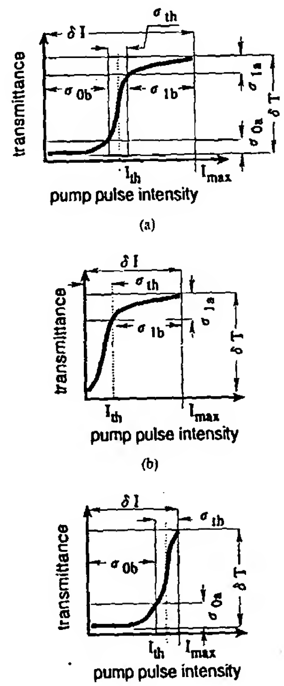

Fig. 5. Performance parameters. (a) Clamping at both "0" and "1" level, (b) clamping at only "1" level, and (c) clamping at only "0" level.

intensity where the differential coefficient of transmittance reaches maximum. σ_{th} is an ambiguity region for discrimination, which we define as the range of pumping intensity in which the transmittance of the gates is 20–80% of their maximum. δT means the total dynamic range in transmittance. For simplicity, we assume the maximum transmittance is unity. Among these parameters, σ_{1b} normalized by I_{max} is important for discrimination. At discrimination, the tail of the probability distribution function over σ_{1b} will not be clamped and will cause errors. Therefore, the optical gates should have σ_{1b} that is large enough ensure the bit error rate is lower than the requirements for the transmission link. Typical requirement for the BER is less than 10^{-15} · η_1, the second parameter is the σ_{1a} (normalized by δT) divided by σ_{1b} (normalized by I_{max}). The η_1 expresses the clamping parameter for the fluctuation of "1" level. The η_1 should be zero for ideal discrimination, which means no fluctuation will transmit to the discriminated signal. In the ideal case, discriminated signal has only the fluctuation of the clock light source, which should have shot noise only. The η_1 of unity means no reduction of fluctuation of the "1" level. These two parameters can be determined for the "0" level in a similar manner.

We cannot determine the parameters for the "0" level when the gate has only limiting characteristics, as shown in Fig. 5(b). On the contrary, we cannot define these parameters for the "1" level when the gate has thresholding characteristics only, as shown in Fig. 5(c).

The third parameter is the extinction ratio ($R_{ext,g}$) of the optical gate. $R_{ext,g}$ is the ratio of the transmittance of the "0" level to "1" level.

D. Calculation of Probability Density Functions

In general, the probability density function (pdf's) of "0" and "1" for signal pulses can be expressed

$$P_{``0"}(n) = \frac{1}{\sigma_0\sqrt{\pi}} e^{(n-n_0/\sigma_0)^2} \tag{1}$$

$$P_{``1"}(n) = \frac{1}{\sigma_1\sqrt{\pi}} e^{(n-n_1/\sigma_1)^2} \tag{2}$$

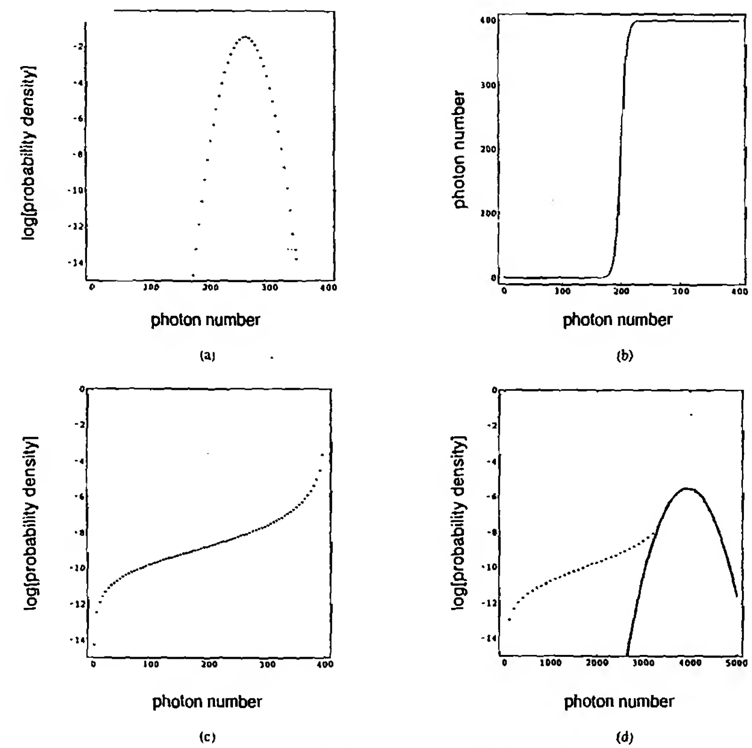

Fig. 6. The pdf's for "1" level before and after discrimination and amplification. (a) Before discrimination, (b) response in transmittance, (c) after discrimination, and (d) discriminated and amplified.

TABLE I
PARAMETER DESCRIPTIONS FOR PDF CALCULATIONS

symbol	meaning
n_0	mean photon number in "0" level
n_1	mean photon number in "1" level
σ_0	variance of photon number in "0" level
σ_1	variance of photon number in "1" level

The parameters are summarized in Table I. In the case of amplification by an optical amplifier, the mean number of amplified photons and its variance can be expressed as

$$\langle n_{out}\rangle = G\langle n_{in}\rangle + 2(G-1)n_{sp}B_{opt} \tag{3}$$

$$\sigma_2 = G\langle n_{in}\rangle + 2(G-1)n_{sp}B_{opt} + 2G(G-1)n_{sp}\langle n_{in}\rangle + 2(G-1)^2 n_{sp}^2 B_{opt}. \tag{4}$$

The parameters are summarized in Table II. The first term in (3) is an amplified signal, and the second term is the spontaneous emission component. The first two terms in (4) express shot noise. The remaining two terms are signal-ASE beat noise and ASE-ASE beat noise components, respectively. By all-optical discrimination, pdf's will be modified depending on the nonlinear threshold response of the optical gate. We assume transmittance $T(n)$ of the gate as the shape shown in Fig. 6(b). The function has a nonlinear threshold change in transmittance.

TABLE II
PARAMETER DESCRIPTIONS FOR PDF CALCULATIONS

symbol	meaning
n_{out}	amplified photon number
n_{in}	input photon number
G	amplifier gain
n_{sp}	inverse population factor
B_{opt}	optical bandwidth of EDFA
σ	variance of amplified photon number

As a result, pdf's of the discriminated "0" and "1" level can be expressed as

$$P^{\rm out}_{\text{"0"}}(n) = P^{\rm in}_{\text{"0"}}[T^{-1}(n)]\left[\left[\frac{dT}{dn_{in}}\right]_{n_{in}=T^{-1}(n)}\right]^{-1} \quad (5)$$

$$P^{\rm out}_{\text{"1"}}(n) = P^{\rm in}_{\text{"1"}}[T^{-1}(n)]\left[\left[\frac{dT}{dn_{in}}\right]_{n_{in}=T^{-1}(n)}\right]^{-1}. \quad (6)$$

In this way, we can calculate the change of pdf's by all-optical discrimination.

We have solved the master equation for discriminated non-Gaussian pdf's, and obtained non-Gaussian amplified pdf's [13]. The pdf's for the "1" level before and after discrimination and after amplification by the EDFA are shown in Fig. 6 with the response of nonlinear optical gate. The mean and variance are far below a real optical signal which has around 10^6 photons per 100 pico second. Because the discriminated pdf's do not have a Gaussian distribution, we cannot characterize the pdf's after discrimination by a mean and variance, which is valid in the case of Gaussian pdf's. In the amplification, the shape of the pdf's are modified and become more Gaussian in shape. This modification can be interpreted as a coherent linear amplification of input pdf's and the addition of Gaussian noise [14], [15]. The main source of this Gaussian noise can be attributed to the well-known signal-ASE beat noise. In Fig. 6(d), we attached a Gaussian distribution profile fitted to the amplified non-Gaussian distribution. The profiles are obtained for very small $\langle n\rangle$ of 3950 photons because of the limited performance of our personal computer. The main part of the pdf fitted in with Gaussian distribution. The difference between these profiles appeared below 10^{-8} of pdf's. 10^{-8} is the value of pdf at the threshold photon number [200 photons in Fig. 6(b)]. In usual condition for optical communication, $\langle n\rangle$ is around 10^6 photons/100 ps (1 mW, 10 Gb/s), and $\langle\sigma\rangle$ is about 10^3. Provided that we set the threshold photon number at $10^6/2$ photons, the deviation from the Gaussian appears below 10^{-10000} of pdf's. Therefore, we can neglect the residual non-Gaussian tail of the amplified signal. For simplification of analysis, we only consider the main Gaussian part of pdf. Under these assumptions, we can formulate the mean photon number and its variance for the "1" and "0" level in front of the final detector.

At the output of optical amplifier α in Fig. 3, we can express the variance of photon number as

$$\begin{aligned}\langle\sigma^2_{\text{"1"}}\rangle_\alpha =& (G_\alpha\langle n_{\text{"1"}}\rangle_{\rm I} + 2(G_\alpha-1)n_{sp}B_{opt}\\ &+ 2(G_\alpha-1)n_{sp}G_\alpha\langle n_{\text{"1"}}\rangle_{\rm I}\\ &+ 2(G_\alpha-1)^2n_{sp}^2B_{opt})\end{aligned} \quad (7)$$

$$\begin{aligned}\langle\sigma^2_{\text{"0"}}\rangle =& (G_\alpha\langle n_{\text{"0"}}\rangle_{\rm I} + 2(G_\alpha-1)n_{sp}B_{opt}\\ &+ 2(G_\alpha-1)n_{sp}G_\alpha\langle n_{\text{"0"}}\rangle_{\rm I}\\ &+ 2(G_\alpha-1)^2n_{sp}^2B_{opt})\end{aligned} \quad (8)$$

where the mean photon number on the "0" level can be written as

$$\langle n_{\text{"0"}}\rangle_{\rm I} = R_{ext,m}\langle n_{\text{"1"}}\rangle_{\rm I}. \quad (9)$$

TABLE III
PARAMETER DESCRIPTIONS FOR PDF CALCULATIONS

symbol	meaning
$\langle\sigma^2_{\text{"1" or "0"}}\rangle_\alpha$	variance of photon number at the output of amplifier α
$\langle n_{\text{"1" or "0"}}\rangle_{\rm I}$	the mean photon number at the input of amplifier α
G_α	gain of amplifier α
n_{sp}	inverse population factor
B_{opt}	optical bandwidth in optical amplifier
$R_{ext,m}$	extinction ratio of modulation in OS
$\langle n_{\text{"1" or "0"}}\rangle_{\rm II}$	the mean photon number at the input of amplifier β
$R_{ext,g}$	extinction ratio of optical gate
$\langle n_{\text{"1" or "0"}}\rangle_{\rm III}$	the mean photon number at the output of amplifier β
$\langle\sigma^2_{\text{"1" or "0"}}\rangle_\beta$	variance of photon number at the output of amplifier β
G_β	gain of amplifier β
$\eta_{\text{"1" or "0"}}$	clamping parameter of optical gate
B	electrical bandwidth of optical detector
erfc	complementary Gaussian error function

The parameters are summarized in Table III. We assume the loss of the optical gate at the "1" level as

$$L_{\tau,\text{"1"}} = 1 \quad (10)$$

for simplicity.

Therefore, the mean photon number at point II can be written as

$$\langle n_{\text{"0"}}\rangle = R_{ext,g}\langle n_{\text{"1"}}\rangle_{\rm II}. \quad (11)$$

In this calculation, we assume that the optical output power of each amplifier is equal and the gain of each amplifier is the inverse of the loss of the attenuator such that

$$G_\alpha\langle n_{\text{"1"}}\rangle_{\rm I}h\nu = G_\beta\langle n_{\text{"1"}}\rangle_{\rm II}h\nu = 1 \text{ mW} \quad (12)$$

$$G_{\alpha,\beta} = 1/L_{\alpha,\beta}. \quad (13)$$

In this case, we assume that the launched optical power for a nonlinear optical gate is 1 mW. A counting time and a measurement bandwidth are 100 ps and 5 GHz (assuming a Nyquist minimum bandwidth), respectively. Finally, we can estimate the mean photon number and variance at the point III in Fig. 3 as

$$\langle n_{\text{"1"}}\rangle_{\rm III} = G_\beta\langle n_{\text{"1"}}\rangle_{\rm II} + 2(G_\beta-1)n_{sp}B_{opt} \quad (14)$$

$$\langle n_{\text{"0"}}\rangle_{\rm III} = G_\beta\langle n_{\text{"0"}}\rangle_{\rm II} + 2(G_\beta-1)n_{sp}B_{opt} \quad (15)$$

$$\begin{aligned}\langle\sigma^2_{\text{"1"}}\rangle_\beta =& G_\beta\langle n_{\text{"1"}}\rangle_{\rm II} + 2(G_\beta-1)n_{sp}B_{opt}\\ &+ (G_\beta-1)n_{sp}G_\beta\langle n_{\text{"1"}}\rangle_{\rm II}\\ &+ 2(G_\beta-1)^2n_{sp}^2B_{opt}\\ &+ \eta^2_{\text{"1"}}\langle\sigma^2_{\text{"1"}}\rangle_{\alpha,\rm beat}\end{aligned} \quad (16)$$

$$\begin{aligned}\langle\sigma^2_{\text{"0"}}\rangle_\beta =& G_\beta\langle n_{\text{"0"}}\rangle_{\rm II} + 2(G_\beta-1)n_{sp}B_{opt}\\ &+ 2(G_\beta-1)n_{sp}G_\beta\langle n_{\text{"0"}}\rangle_{\rm II}\\ &+ 2(G_\beta-1)^2n_{sp}^2B_{opt} + G_\beta\\ &+ \eta^2_{\text{"0"}}\langle\sigma^2_{\text{"0"}}\rangle_{\alpha,\rm beat}.\end{aligned} \quad (17)$$

The first four terms in (16) and (17) resulted from there being an optical amplifier in the receiver. The remaining terms are excess noise components imposed by the optical amplifier before discriminator. The derivation of those terms is described in Appendix.

Assuming the quantum efficiency is unity, we can evaluate the Q factor at final detection as follows:

$$Q = \frac{\langle n_{\text{"1"}}\rangle^{\rm elec}_{\rm III} - \langle n_{\text{"0"}}\rangle^{\rm elec}_{\rm III}}{\langle\sigma_{\text{"1"}}\rangle^{\rm elec}_\beta + \langle\sigma_{\text{"0"}}\rangle^{\rm elec}_\beta} \quad (18)$$

$$\langle n_{\text{"1"},\text{"0"}}\rangle^{\rm elec}_{\rm III} = \langle n_{\text{"1"},\text{"0"}}\rangle_{\rm III} \quad (19)$$

$$\langle\sigma_{\text{"1"},\text{"0"}}\rangle^{\rm elec}_\beta = \sqrt{2B}\langle\sigma_{\text{"1"},\text{"0"}}\rangle_\beta. \quad (20)$$

Provided that we set the decision level to an optimum value determined by

$$\langle n_{\rm th}\rangle^{\rm elec} = \frac{\langle\sigma_{\text{"0"}}\rangle^{\rm elec}_\beta\langle n_{\text{"1"}}\rangle^{\rm elec}_{\rm III} + \langle\sigma_{\text{"1"}}\rangle^{\rm elec}_\beta\langle n_{\text{"0"}}\rangle^{\rm elec}_{\rm III}}{\langle\sigma_{\text{"0"}}\rangle^{\rm elec}_\beta + \langle\sigma_{\text{"1"}}\rangle^{\rm elec}_\beta} \quad (21)$$

the bit error rates can be calculated by the Q values easily as

$$\mathrm{BER} = \frac{1}{2}\,\mathrm{erfc}\left(\frac{Q}{\sqrt{2}}\right). \quad (22)$$

E. Results of Estimation

According to the model and conditions, we calculated the Q values and the bit error rate of discriminated and amplified signal. Fig. 7 shows calculated Q values as a function of η. Assumed parameters are summarized in Table IV. When η is unity, optical discrimination has no effect and ASE noise generated by the first amplification contributes to the degradation of the Q values as a whole. But the contribution is reduced for small η. When η equals zero discrimination is complete, and any contribution to the degradation from amplifier α is completely eliminated. The resulting Q values stay high for small η. Naturally, both "1" and "0" level clamping is the most effective. As shown clearly in Fig. 7, clamping at "1" level only is more effective than at "0" level only. This difference can be attributed to the fact that the dominant noise source is a signal-ASE beat noise component, which is mainly imposed on the "1" level distribution. Fig. 8 shows the calculated bit error rate performances by optical discrimination. Assumed parameters are the same as the calculation in Fig. 7, but the optical input power to the OR is changed. The power penalty is effectively reduced by optical discrimination. We have carried out all-optical discrimination experiment to confirm these qualitative estimations.

IV. Ultrafast Nonlinear Gate: LOTOS

A. Structure and Basic Operation

Fig. 9 shows the schematic structure of the LOTOS. The LOTOS comprises an anti-reflection film layer, an InP substrate, an InGaAsP/InP distributed Bragg reflector (DBR) layer, a Be-doped low-temperature-grown strained InGaAs/InAlAs multiple quantum-well (MQW) layer, and an Au mirror layer. Amplified signal pulses as shown in Fig. 2 open the optical gate by a bleaching of exciton absorpti[on] of the MQW layer (ON state). Optical clock pulses th[e]

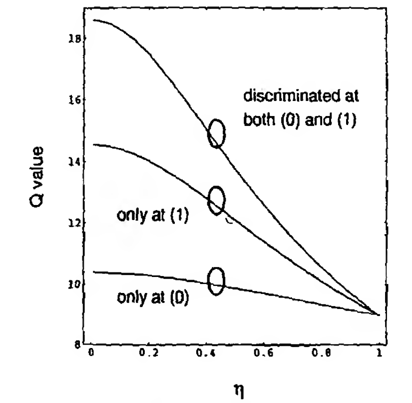

Fig. 7. Calculated Q value by optical discrimination.

TABLE IV
PARAMETER DESCRIPTIONS FOR Q-VALUE ESTIMATIONS

parameter	value
bitrate	10 GHz
optical bandpass filter bandwidth	100 GHz
n_{sp}	1
gain of optical amplifier	32 dB
extinction ratio of modulator	10 dB
extinction ratio of optical gate	10 dB
optical input power for optical receiver	- 27 dBm

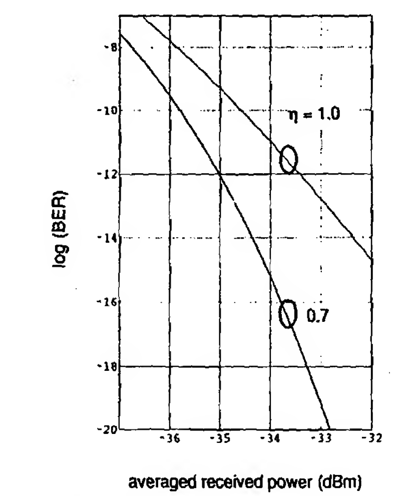

Fig. 8. Calculated BER's at optical discrimination.

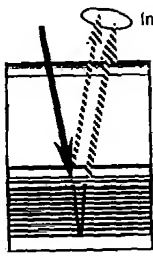

Fig. 9. Structure of LOTOS.

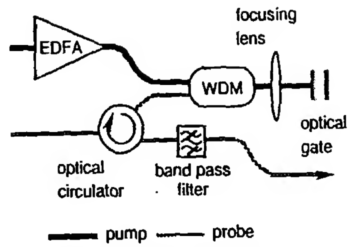

Fig. 10. Experimental setup for LOTOS evaluation.

synchronized to the signal pulses pass through the gate by the instantaneous increase of transmittance. Without pumping signal pulses, all the clock pulses are absorbed in the MQW layer (OFF state). The DBR mirror was designed so that the amplitude reflectivity is equals to the value that cancel the leaked light from the MQW layer in OFF state, and the phase has a relative difference of $(2n-1)\pi$ $\{n:\text{integer}\}$ against the leaked light. Consequently, the leaked light destructively interferes with the light reflected by the DBR mirror. Therefore, the extinction ratio can be improved by the interference effect. We will discuss the effect of the DBR mirror in Chapter VI.

B. Advantages and Disadvantages of LOTOS

The advantages of LOTOS are transmittance nonlinearity suitable for discrimination, ultrashort carrier lifetime, and a wide wavelength range for operation. LOTOS has ultrashort carrier relaxation time, which can be controlled from several hundred fs to tens of ps, and a nonlinear change in transmittance due to the saturation of exciton absorption. Moreover, a high extinction ratio was achieved by using the DBR mirror layer. The operating wavelength range is as wide as 30 nm as a result of the bandwidth of the exciton absorption.

The LOTOS has a polarization dependence originating from the switching mechanism. The relaxation time between two excited spin states which correspond to two circular polarization states of pumping pulse, is several tens of ps. This is substantially longer than the carrier relaxation time of several ps. Therefore, the switching characteristics depend on the polarization state of pump pulses. One way to avoid this dependence is to pump with linearly polarized light. A linearly polarized light is equivalent to circulary polarized light in 50% of clockwise and counterclockwise directions. Accordingly, there is no polarization dependency for the probe light.

C. Evaluation of LOTOS Switching Characteristics

Pump and probe pulses were coupled by a wavelength division multiplexing (WDM) coupler and focused on LOTOS by a lens with a numerical aperture (NA) of 0.7. The temporal transmission response of the optical gate was observed with a streak camera having resolution of 2 ps. We used a mode-locked laser diode (MLLD) [16] monolithically integrated with electro-absorption optical intensity modulator to generate pump pulses with 3–6 ps pulse width and gain switched laser to generate pulses with 10–12 ps width. Wavelengths were 1534.5 and 1565.0 nm for pump and 1530–1570 nm for probe. Probe pulse sources were a 1553-nm gain switched laser diode or a 1552-nm mode-locked laser diode that has the same structure as the pump pulse sources. The experimental setup is shown in Fig. 10.

For the measurement of temporal transmittance, we used a 1552-nm continuous wave (CW) light source as the probe light. The extinction ratio of the gate was estimated by the ratio of the intensity of the gated pulse in the OFF state to their intensity in the ON state, which were measured by a streak camera. The linearity of the response of the streak camera was calibrated by measuring the response count for optical pulses of known intensity. The maximum extinction ratio that can be measured by the method is about 15 dB. Transmittance was obtained by calculating the ratios of the intensity of the reflected probe pulses to the intensity of input probe pulses measured by an optical power meter. Isolation of probe light from pump light was more than 30 dB due to the use of an optical band pass filter.

Fig. 11(a) and (b) shows transmittance of the gate against pump pulse energy, respectively. The transmittance increase with increasing pump pulse energy. Transmittance has non-linearity and abruptly increases at the threshold pump pulse energy [Fig. 11(b)]. Saturation of transmittance was observed at high pump pulse energies. The estimated value of η is 0.57 for the 1-μm thick LOTOS. Therefore, effective discrimination performance can be expected.

Fig. 12 shows a streak camera trace of measured temporal transmittance. We have obtained a short response time of 14 ps. The probe wavelength dependence of the extinction ratio was measured by changing the wavelength of the CW light source, and the results are shown in Fig. 13. The extinction ratio stayed at 10 dB under a wide wavelength range of about 10 nm and reached the maximum at 1552 nm. Therefore, we set the pump and a probe wavelengths to 1565 and 1552 nm, respectively, in the optical discrimination experiments, which will be discussed later.

V. Experimental Results

A. Experimental Setup for Discrimination

The experimental setup is shown in Fig. 14. We generated optical signal pulses encoded in a 31-stage pseudorandom binary sequence (PRBS) by MLLD and lithium niobate (LN) optical intensity modulator. Local clock pulses were generated by another MLLD, which was synchronized with signal pulses using the same reference oscillator. Wavelengths of the signal pulses and the clock pulses are 1565 and 1552 nm, respectively. Pulse widths measured by the streak camera are 6 ps full-width at half-maximum (FWHM) for both. We set the optical pump pulse energy to 1–2 pJ for pumping and 1×10^2 fJ for the probe pulse to prevent gating by the energy of the probe pulse. That is, optical gating was achieved solely by pump pulses.

Discriminated signal pulses are separated by the same WDM coupler used at combining, and an additional optical band-pass filter of 3 nm FWHM was used to increase isolation from reflected pump pulses. No less than 30 dB isolation was achieved.

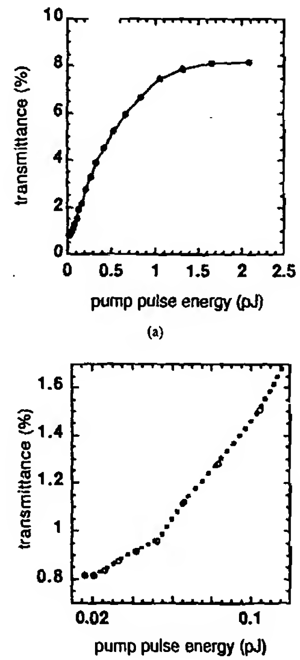

Fig. 11. Response of LOTOS. (a) Transmittance of LOTOS and (b) transmittance of LOTOS at lower pumping energy.

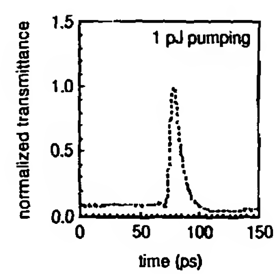

Fig. 12. Temporal gating profile.

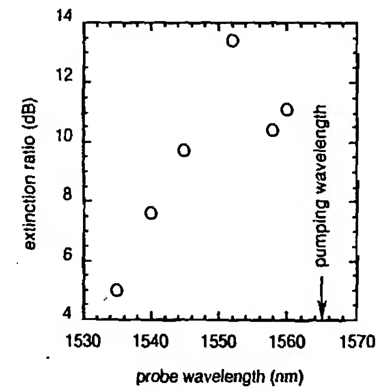

Fig. 13. Extinction ratio versus probe wavelength.

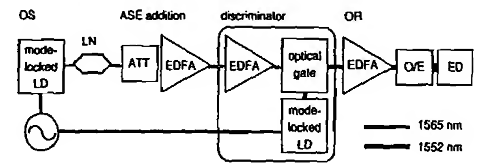

Fig. 14. Experimental setup for the discrimination.

B. Discrimination Performance for ASE Noise

We examined the optical discriminator's tolerance against ASE noise by changing the amount of ASE noise added to the optical signal and extinction ratio recovery by detuning the bias voltage of LN modulator. Measured repetition frequencies were 0.6, 2.4, and 10 GHz. Thickness of the MQW layer in the LOTOS were 4, 2, and 1.2 μm.

First, we investigated the improvement of extinction ratio by optical discriminator. Fig. 15(a) shows the bit error rate before and after discrimination at 0.6 Gbit/s. We intentionally degraded an extinction ratio of optical signal by detuning the bias voltage of LN modulator. The power penalty induced by the extinction ratio degradation was clearly suppressed. Then we examined the ASE noise reduction performance of the discriminator. Fig. 15(b) shows the bit error rate and eye diagrams before and after discrimination at 2.4 Gb/s. We measured bit error rates for optical signal pulses generated by the clock pulse source and LN modulator, for ASE added optical signal pulses, and for the discriminated signal pulses, which were ASE added in advance. The receiver sensitivity for the bit error rate of 10^{-9} after discrimination was 3 dB higher than before. The eye diagrams clearly indicate a reduction of ASE originated noise before and after discrimination. These results confirm the qualitative estimation of optical discriminator. Dependence of the sensitivity on pattern length

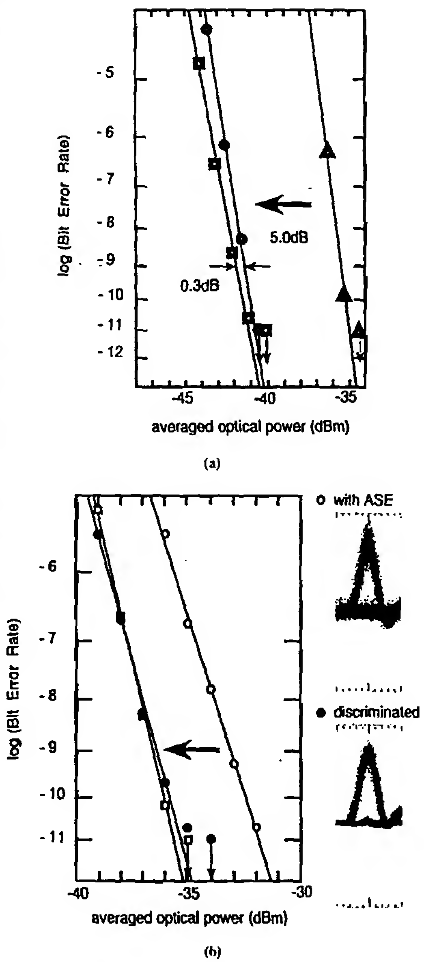

Fig. 15. Bit error rate performance for discrimination. (a) BER at 622 Mb/s PRBS 23 and (b) BER at 2.4 Gb/s PRBS 23 with eye diagrams.

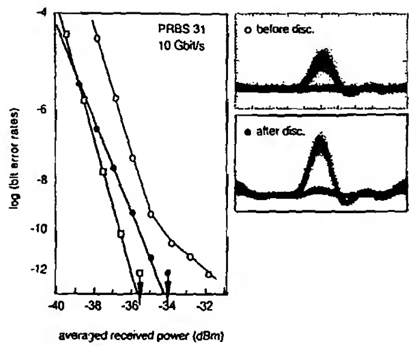

Fig. 16. Bit error rate performance for 10 Gb/s operation.

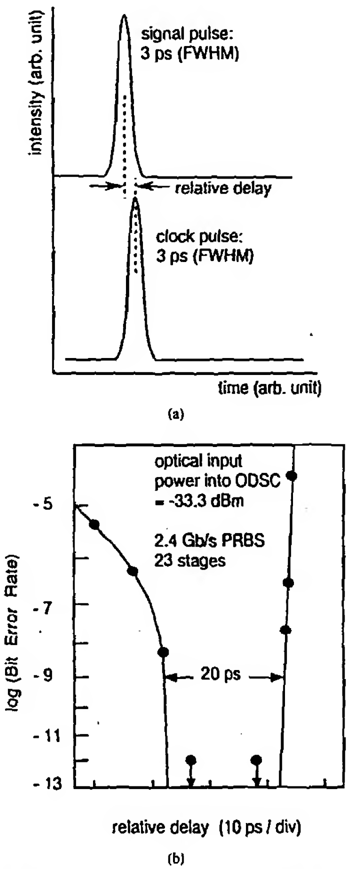

Fig. 17. Phase margin of ODSC. (a) Relative delay and (b) temporal tolerance.

of the PRBS in the range of 7–23 stages was not observed in discrimination experiment. Fig. 16 shows the result of an equivalent experiment at 10 Gb/s using a 1-μm thick MQW. The regeneration of the SNR by optical discrimination was confirmed at 10 Gb/s.

C. Jitter Tolerance

As we pointed out in Section II, jitter tolerance for this discriminator is an important feature. Therefore, we investigated the temporal tolerance between pumping signal pulses and clock pulses. We measured the bit error rate changing the relative delay between signal and clock pulses as shown in Fig. 17(a). Temporal tolerance of 20 ps (18° for 2.4 Gb/s) was obtained at the bit error rate of 10^{-9} [Fig. 17(b)]. Therefore, timing jitter less than 20 ps can be reduced effectively.

Discussion

A. Nonlinearity and Other Optical Gates

The nonlinearity of optical gates is the key characteristic as we have pointed out in Section III. As for LOTOS, we have obtained an η value of 0.57, which is effective for all-optical discrimination. Other optical gates, such as NOLM-based gates [1]–[2], have a cosine-like profile in principle. If we apply the same definition of η to those gates, the estimate η value is 0.54. Therefore, we can expect similar discrimination performances for these gates from the viewpoint of the nonlinearity of optical transmittance. The switching energy for LOTOS is around 1 pJ, which was less the value for NOLM optical gates. The gating window of LOTOS is 14 ps, but the value can be reduced to several hundred fs by controlling of the Be-doping level. The intrinsic response time of Kerr nonlinearity, which governs the response time of NOLM-based optical gates is several fs. The operating wavelength range is about 30-nm for LOTOS. NOLM gates suffer severe restrictions on operating wavelength in principle. The actual size of LOTOS are about several cm, including the focusing optics. In comparison, NOLM are large, and have a long switching fiber and a large signal latency. LOTOS gates are quite stable under temperature fluctuations. But NOLM gates need temperature stabilization for normal operation. This is especially true for gates, which require severe temperature control for the switching fibers.

In summary, the advantages of LOTOS are nonlinearity in transmittance, a wide operating wavelength range, an ultra short gating window, low switching energy, compactness, and stability.

B. Repetition Limit of LOTOS

The maximum repetition frequency of LOTOS is limited by the degradation of the transmittance of the optical gate. The degradation can be attributed to the thermal red shift of the absorption edge of the MQW.

Since the optical gate absorbs pumping optical power, absorbed power increases the temperature of the MQW. This could cause severe problems, such as the red shift of the absorption edge. The red shift could bring about extra-absorption, which would make the transmittance decrease considerably. Therefore, we have to suppress the temperature rise as much as possible.

The amount of absorbed optical power, and the heat resistance and heat capacity of the MQW are dominant factors affecting the temperature rise. Fig. 18 shows the calculated temperature rise at pump-irradiated spot as a function of averaged pumping power. The calculated temperature rise at the pumping power of 10 mW (1 pJ at 10-GHz repetition frequency) is 25 K for a 1-μm thick optical gate. Such a rise can cause a severe red shift of the absorption edge [18].

This thermal effect was observed experimentally. Fig. 19 shows the transmittance of a 2-μm thick gate as a function of pump pulse energy for several repetition frequencies. Averaged pumping power is 1.2 mW at 2 pJ of pump pulse energy and 600-MHz repetition frequency. No degradation of transmittance was observed (square), but transmittance

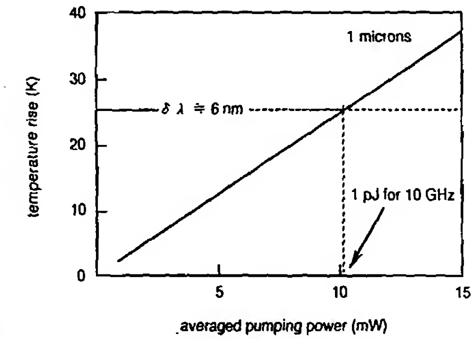

Fig. 18. Calculated temperature rise.

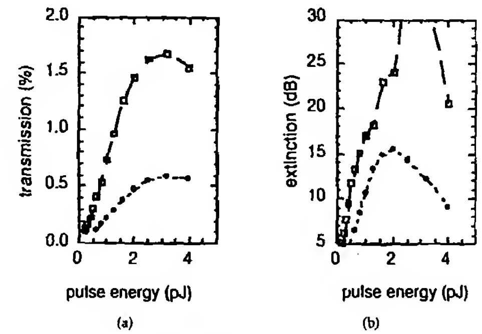

Fig. 19. Thermal degradation of LOTOS.

TABLE V
PARAMETER DESCRIPTIONS FOR SWITCHING ENERGY ESTIMATION

symbol	*meaning*
V	volume concerning a switching
N_c	carrier density needed for absorption saturation
h	Plank constant
c	velocity of light
λ	wavelength of pumping light

severely degraded at pumping powers above 10 mW at 5-GHz repetition frequency (circle). This degradation could be attributed to the red shift at the absorption edge.

Reduction of switching energy is effective in suppressing the temperature rise. Switching energy is proportional to a volume concerning the saturation of absorption, and can be expressed as

$$E_{sw} = VN_c\frac{hc}{\lambda}. \tag{23}$$

The parameters are summarized in Table V. Fig. 20 shows the calculated switching energy (E_{sw}). Experimental values are plotted as a function of MQW thickness. The refractive

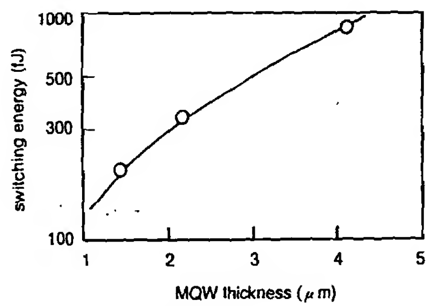

Fig. 20. Switching energies of LOTOS.

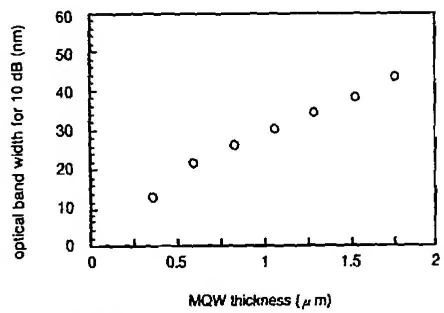

Fig. 21. Optical bandwidth versus MQW thickness.

index of the MQW layer is assumed to be 3.3. The volume (V) is a function of the irradiating spot radius and MQW layer thickness. The carrier density (N_c) required for a saturation of absorption is assumed to be 5×10^{17} cm^{-3}. Experimental E_{sw}'s are defined as the pump pulse energy required to achieve a 10-dB extinction ratio, and they agree well with calculated values. This means, we have succeeded in the reduction of a switching energy. The reduction of E_{sw} relaxes the degradation of transmittance and enables 10 Gb/s operation. Further improvement of repetition frequency is expected by reducing E_{sw}, improving heat transfer, and cooling the MQW.

C. Optical Bandwidth of LOTOS

We define the optical bandwidth of LOTOS as the wavelength range in which a high extinction ratio is maintained. The bandwidth is determined by MQW thickness and the absorption coefficient in the OFF state.

As we pointed out in Section IV-A. The DBR mirror layer is designed so that the intensity of reflected light from the DBR is equal to the intensity of light leaking from unsaturated MQW and so that the relative phase difference between the two light waves is $(2n-1)\pi$ ($n = 1, 2, 3, \cdots$). Provided that the thickness of MQW and absorption coefficient in the OFF state are given, we can calculate the optimum reflectivity for the maximum extinction ratio.

As we increase DBR reflectivity, multiple reflection of the light wave between the DBR and Au mirror will be effective in the ON state. Therefore, the optical bandwidth of high extinction ratio will decrease by this cavity effect. In other word, a Fabry–Perot cavity will be formed between the two layers. Fig. 21 shows the calculated bandwidth for more than a 10-dB extinction ratio. As we reduce MQW layer thickness, the bandwidth decreases. The bandwidth is 30 nm for a 1-μm thick MQW.

Even in the ON state, the gated light wave will be partially eliminated by destructive interference with the light wave reflected by the DBR mirror. The degradation of transmittance can be treated as an extra insertion loss. Fig. 22 shows the insertion loss as a function of MQW thickness. We optimized the reflectivity of the DBR mirror for each thickness in the calculation. The insertion loss increases with decreasing MQW thickness. In order to ensure the insertion loss is no more than

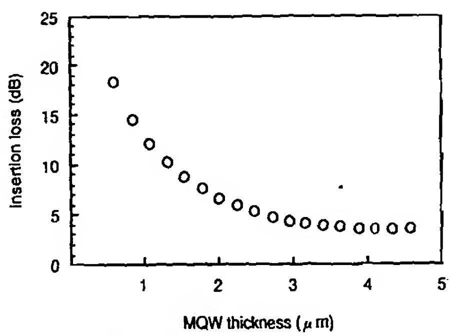

Fig. 22. Insertion loss versus MQW thickness.

15 dB, the thickness of MQW layer should be no less than 1 μm. The optimized reflectivity is 13% for 1 μm.

D. No Wavelength Change Configuration

LOTOS is a surface-reflection-type optical gate. Therefore, we can separate the pump and probe pulses by their spatial trajectory using multiple input–output port lenses. Each isolated lens has the same focusing spots. Pump and probe lays have their own isolated trajectory but the same spot on the optical gate. Therefore, we can use the same wavelength for pump and probe pulses. There is no need for WDM couplers, optical band pass filters, or fiber Bragg gratings for channel separation. Because we have to share the N.A. for input/output ports, the maximum effective N.A. must be smaller than that for the single port WDM configuration. For optical regenerative repeaters, the wavelength of pump and probe pulses should be the same to achieve cascadability of regenerators. Therefore, it is important to realize the multiport optics.

VII. Conclusion

We proposed an all-optical discriminator having a nonlinear optical gate, and introduced performance parameters to quantify the discrimination performance of the gates. The clamping parameter η primarily determine the discrimination performance. The η value for existing optical gates, such

as NOLM and LOTOS were estimated to be about 0.6. A simplified theoretical estimation using the parameters revealed that the discriminator can regenerate optical signal pulses and consequently suppress the ASE-noise-induced degradation of SNR sufficiently with the η values. In the estimation, the clamping at the "1" (mark) level of pdf's was more effective for recovery of SNR than at the "0" (space) level in the usual case where signal-ASE beat noise is a dominant noise source. We examined the discrimination performance experimentally utilizing the MQW optical gate, and confirmed the suppression by the reduction of the ASE-noise-induced power penalty at 0.6, 2.4, and 10 Gbit/s.

Appendix

We define γ as

$$1+\gamma \equiv \frac{\langle\sigma^2\rangle_{II}}{\langle n\rangle_{II}} \tag{A-1}$$

where γ degradation coefficient of light input to amplifiers. γ equals to zero means a coherent state. Therefore, the excessive noise component can be expressed as

$$G_\beta^2\gamma\langle n\rangle_{II} = G_\beta^2(\langle\sigma^2\rangle_{II} - \langle n\rangle_{II}). \tag{A-2}$$

Here, the variance of the input of amplifier β can be expressed by discrimination parameter η, optical loss of the attenuator β and the beat components in the output variance of amplifier α [the third and fourth term of (7) and (8)] as

$$\langle\sigma^2\rangle_{II} = [\eta L_\beta\langle\sigma\rangle_{\alpha,\text{beat}}]^2 + \langle n\rangle_{II}. \tag{A-3}$$

$$\langle\sigma\rangle_{\alpha,\text{beat}} = \sqrt{\langle 2(G_\alpha-1)n_{sp}G_\alpha\langle n\rangle_I + 2(G_\alpha-1)^2n_{sl}^2B_{\text{opt}}\rangle}. \tag{A-4}$$

Since amplifier β compensates for the loss of optical attenuator β, the value of the loss coincides with the optical gain of the amplifier. Therefore

$$L_\beta = \frac{1}{G_\beta}. \tag{A-5}$$

Combining (A-2), (A-3), and (A-5),

$$G_\beta^2\gamma\langle n\rangle = \eta^2\langle\sigma^2\rangle_{\alpha,\text{beat}}. \tag{A-6}$$

References

[1] K. Smith, and J. K. Lucek, "All-optical signal regenerator," in *Proc. CLEO'93*, vol. CPD23, 1993, pp. 1/46–2/47.
[2] M. Jinno and M. Abe, "All-optical regenerator based on nonlinear fiber sagnac interferometer," *Electron. Lett.*, vol. 28, pp. 1350–1352, 1992.
[3] A. Dupas, L. Billes, J. C. Simon, B. Landousies, M. Henry, F. Ratovelomanana, A. Enard, and N. Vodjdani, "Progress toward a pan-european WDM network: 3600 km, 2.5 Gbit/s cascade of all optical 2R regenerator/wavelength converters and 400 km uncompensated standard fiber sections," in *Proc. ECOC'97*, vol. 5, 1997, pp. 85–88.
[4] D. Chiaroni, B. Lavigne, A. Jourdan, L. Hamon, C. Janz, and M. Renaud, "New 10 Gbit/s 3R NRZ optical regenerative interface based on semiconductor optical amplifiers for all-optical networks," in *Proc. ECOC'97*, vol. 5, 1997, pp. 41–44.
[5] R. Takahashi, Y. Kawamura, T. Kagawa, and H. Iwamura, "Ultrafast 1.55-μm photoresponses in low-temperature-grown InGaAs/InAlAs quantum wells," *Appl. Phys. Lett.*, vol. 65, pp. 1790–1792, 1994.
[6] R. Takahashi, Y. Kawamura, and H. Iwamura, "1.55 micro meter ultrafast surface-reflection all-optical switching using low-temperature-grown Be-doped strained MQW's," in *Proc. ECOC'94*, 1994, pp. PD113–116.
[7] H. Kobayashi, R. Takahashi, Y. Matsuoka, and H. Iwamura, "Ultrafast all-optical switch using low-temperature-grown InGaAs/InAlAs multiple quantum well," in *Proc. 4th Int. Workshop Femtosecond Technol.*, 1997, pp. 28–30.
[8] H. Kurita, T. Shimizu, and H. Yokoyama, "All-optical clock extraction at bit rates up to 80 Gbit/s with monolithic mode-locked laser diodes," in *Proc. CLEO'97*, vol. CTuJ5, 1997.
[9] O. Kamatani, S. Kawanishi, and M. Saruwatari, "Prescaled 6.3 GHz clock recovery from 50 Gbit/s TDM optical signal with 50 GHz PLL using four-wave mixing in a traveling-wave laser diode optical amplifier," *Electron. Lett.*, vol. 30, pp. 807–809, 1994.
[10] H. Tsuda, A. Hirano, R. Takahashi, K. Sato, and K. Hagimoto, "All-optical pulse discrimination experiment using a low-temperature-grown multiple quantum well optical switch," *Electron. Lett.*, vol. 32, pp. 365–366, 1996.
[11] A. Hirano, H. Tsuda, K. Hagimoto, R. Takahashi, Y. Kawamura, and H. Iwamura, "10 ps pulse all-optical discrimination using a high-speed saturable absorber optical gate," *Electron. Lett.*, vol. 31, pp. 736–737, 1995.
[12] A. Hirano, H. Kobayashi, H. Tsuda, R. Takahashi, M. Asobe, K. Sato and K. Hagimoto, "10-Gbit/s RZ all-optical discrimination using a refined saturable absorber optical gate," *Electron. Lett.*, vol. 34, pp. 198–199, 1998.
[13] M. Jinno, "Effects of crosstalk and timing jitter on all-optical time-division demultiplexing using a nonlinear fiber sagnac interferometer switch," *IEEE J. Quantum Electron.*, vol. 30, pp. 2842–2853, 1994.
[14] K. Shimoda, H. Takahasi, and C. H. Towns, "Fluctuations in amplification of quanta with application to maser amplifiers," *J. Phys. Soc. Japan*, vol. 12, pp. 686–700, 1957.
[15] S. Carusotto, "Quantum statistics of light after one-photon interaction with matter," *Phys. Rev. A*, vol. 11, pp. 1629–1633, 1975.
[16] E. B. Rockower, N. B. Abraham, and S. R. Smith, "Evolution of the quantum statistics of light," *Phys. Rev. A*, vol. 17, pp. 1100–1112, 1978.
[17] K. Sato, I. Kotaka, Y. Kondo, and M. Yamamoto, "Actively mode-locked strained-InGaAsP multiplequantum-well lasers integrated with electroabsorption modulators and distributed Bragg reflectors," in *Proc. OFC'95*, 1995, vol. TuI2, pp. 37–38.
[18] T. Ishibashi, "Gallium arsenide and related compounds," *Oiso*, 1981, p. 587.

Akira Hirano, photograph and biography not available at the time of publication.

Hiroyuki Tsuda, photograph and biography not available at the time of publication.

Hideki Kobayashi, photograph and biography not available at the time of publication.

Ryo Takahashi, photograph and biography not available at the time of publication.

Masaki Asobe, photograph and biography not available at the time of publication.

Kenji Sato, photograph and biography not available at the time of publication.

Kazuo Hagimoto, photograph and biography not available at the time of publication.